Example-Based Assisting Approach for Pulmonary Nodule Classification in 3-D Thoracic CT Images

Yoshiki Kawata[1], Noboru Niki[1], Hironobu Ohmatsu[2], Noriyuki Moriyama[3]
[1] Dept. of Optical Science, Univ. of Tokushima, Tokushima, 770-8506, Japan
{kawata, niki}@opt.tokushima-u.ac.jp
[2]National Cancer Center East Hospital, Chiba, Japan
[3]National Cancer Center Hospital , Tokyo, Japan

Abstract. This paper describes an example-based assisting approach for classifying pulmonary nodules in 3-D thoracic CT images. In this approach the internal and surrounding structures of the nodule are characterized by the distribution pattern of CT density and 3-D curvature indexes. Each nodule is represented by means of a joint histogram using the distance value from the nodule center. When given an indeterminate nodule image, the images of lesions with known diagnoses (e.g. malignant vs. benign) are retrieved from a 3-D nodule image database. The malignant likelihood of the indeterminate case is estimated by the difference between the representation patterns of the indeterminate case and the retrieved lesions. In the present study, we adopt the Mahalanobis distance as the difference measure and then, explore the feasibility of the classification based on patterns of similar lesion images.

1 Introduction

The detection rate of small pulmonary nodules has recently increased due to the advances in imaging technology [1]. It is important to increase the positive predictive value (i.e. ratio of the number of lung cancers found to the total number of biopsies) without reducing the sensitivity of lung cancer detection. Computer-aided diagnosis (CAD) has the potential to increase the diagnostic accuracy by reducing the false-negative rate while increasing the positive predictive values of abnormalities in three-dimensional (3-D) thoracic images. The interpretation of the pulmonary nodule images often involves the matching features extracted from a database of the nodules with associated clinical information. When the matching procedure is performed well, the database can provide physicians with more information concerning the diagnosis and prognosis of the queried nodule. Moreover, the corresponding structures retrieved from the database may help to design the CAD scheme for the distinction between benign and malignant nodules.

In this paper, we formulate the nodule-classification problem as one of learning to recognize nodule patterns from examples. Each nodule pattern is represent by the extracted internal and surrounding features based on CT density and 3-D curvature indexes. We use a database of nodule images to search similar malignant and benign lesion patterns and construct a distribution-based local lesion model in a high-

T. Dohi and R. Kikinis (Eds.): MICCAI 2002, LNCS 2488, pp. 793–800, 2002.

dimensional image vector space of the nodule representation. We then estimate the likelihood of the malignancy by computing the difference between representation patterns of the indeterminate case and the retrieved lesions. We first describe the representation method used as a pre-process of the data and then give the definition of the similarity criteria. We are then showing results of similar nodule images and estimation the malignant likelihood.

2 Materials and Methods

2.1 3-D Nodule Data

The 3D chest image used in this paper was a stack of thin-section CT images obtained by the helical CT scanner (Toshiba TCT900S Superhelix and Xvigor). The thin-section CT images were measured under the following conditions; beam width: 2mm, table speed: 2mm/sec, tube voltage: 120kV, tube current : 250mA or 200mA. The range of pixel size in each square slice of 512 pixels was between 0.3x0.3 mm^2 and 0.4x0.4 mm^2, and the slice contains an extended region of the lung area. The 3D chest image was reconstructed from the thin-section CT images by a linear interpolation technique to make each voxel isotropic. The data set in this study included 263 3-D chest images from 263 patients provided by National Cancer Center Hospital East, Tochigi Cancer Center, and Kanagawa Cancer Center. Of the 263 cases, 194 contained malignant nodules, and 69 contained benign nodules.

2.2 Nodule Representation

We build a 3-D nodule image database from the data set. The database consists of two types elements, such as text-based elements and image-based elements. The text-based elements of the database are as follows, ID number, measurement conditions, sex, age, diagnosis result, nodule diameter and volume that compute from the segmented nodule image. The image-based elements are as follows, the 3-D ROI image with a nodule of interest, the segmented nodule image, the representation of local density pattern inside the nodule and nodule surroundings. Since the internal and surrounding structures of the nodule are important cues to distinct malignancy from benign cases, we concentrate on the feature representation inside the nodule and the nodule surroundings. As pre-processing of the 3-D nodule image database, we perform the following nodule segmentation, feature extraction, and representation procedures.

2.2.1 Segmentation of the nodule and its surroundings

The segmentation of the 3D pulmonary nodule image consists of three steps [2]; 1) extraction of lung area, 2) selection of the region of interest (ROI) including the nodule region, and 3) nodule segmentation based on a deformable surface approach.

The ROI including the nodule was selected interactively. A pulmonary nodule was segmented from the selected ROI image by the deformable surface approach. The nodule surrounding region was computed by the distance from the nodule surface. The distance was obtained by applying the Euclidean distance transformation approach proposed by Saito et al. [6] to the nodule surrounding region.

2.2.2 Feature extraction

Each voxel in the region of interest (ROI) including the pulmonary nodule is locally represented by CT density and curvature index. By assuming that each voxel in the ROI lies on the surface which has the normal corresponding to the 3-D gradient at the voxel, we computed directly the curvatures on each voxel from the first and the second derivatives of the gray level image of the ROI. At each voxel two principal curvatures and directions of principal curvatures are computed by using the approach proposed by Thirion [3]. As the curvature index at each voxel in the ROI image, we use the shape index that is computed from two principal curvatures [4],[5]. The continuous surface type is mapped on the interval [0, 1] of the shape index value.

To quantify the relationship between the nodule and its surrounding structure such as vessel and pleura, we focus on two indicators of malignancy, which are denoted as vascular convergence and pleural retraction. In the 3-D thoracic CT images, these findings are observed so that the vessel and pleura images are drawn in the nodule. We assumed that the shape of the vessel and the pleura images are similar to cylindrical or conic structures. Therefore, we measure an amount of the vascular convergence and pleural retraction by computing the absolute value of the inner product of the directions of cylindrical or conic structures and the normal directions of the nodule surface. For the representation of the directions, we compute two vector fields that consist of the directions of the maximum principal curvature and normal vector of the nodule surface. The vector field is denoted as the maximum principal curvature vector (MPV) field. The normal directions of the nodule surface at the vicinity of the nodule are estimated by a diffusion procedure proposed by Xu [7]. The approach is to keep the desirable property of the gradients near the nodule edges, but to expand the gradient away from the edges into homogeneous regions of the nodule surrounding using the computational diffusion process. The vector field obtained by the normal vector of the nodule surface is denoted as gradient vector (GV) field.

2.2.3 Joint-histogram based representation

In order to characterize the distribution pattern of the CT density and the shape index inside nodule, we compute two types of joint histogram using the distance value from the nodule center. Since the distance value depends on the nodule size, the first type is directly derived from the distance value and used to search similar lesions. Once obtained similar lesions, the variation of internal structure provides more important information to classify nodule patterns rather than the nodule size. Therefore, the second type is derived from the normalized distance value which ranges between zero and one value and used to evaluate the likelihood of the malignancy. To compute the distance value at each voxel, we apply the Euclidean distance transformation technique [6] to the segmented nodule image and obtain the maximum distance value

(D_M) inside the nodule. Since the distance value (v_d) at each voxel is the distance from the nodule surface, the maximum distance value seems to be assigned to the voxel at the nodule center area. To obtain the distance from the nodule center, we compute the value (D_M - v_d) at each voxel inside the nodule. Let $I(\mathbf{x})$ and $D(\mathbf{x})$ be respectively the CT density value and the distance value at the voxel $\mathbf{x}$ in the nodule image. The first type of joint histogram of $I(\mathbf{x})$ and D($\mathbf{x}$) is expressed as

$$H(d_1 = \frac{k_1}{B_1}, d_2 = \frac{k_2}{B_2}) = \frac{1}{N}\sum_{i=1}^{N} K_{k_1,k_2}(I(\mathbf{x}_i), D(\mathbf{x}_i)) \quad (1)$$

with

$$K_{k_1,k_2}(t_1,t_2)\begin{cases} 1 & \frac{k_1-1}{B_1} \le t_1 < \frac{k_1}{B_1}, \frac{k_2-1}{B_2} \le t_2 < \frac{k_2}{B_2} \\ 0 & otherwise \end{cases} \quad (2)$$

where B_1 and B_2 are the numbers of bins for the CT density value and the distance value, respectively, and N is the number of voxels inside the nodule. Statistically, the normalized joint histogram denotes the joint probability of the CT density value and the distance value. It measures how the CT density value distributes inside the nodule with respect to the distance from the nodule center. The similar equation for the first type of joint histogram of the shape index value and the distance value is obtained. In the preliminary study, the domain of CT density, distance value, and shape index values were specified to [-1000, 500] (HU), [0, 50] (voxels), [0, 1], respectively. The number of bins was set to 50 for each value. The second type of joint histograms is computed by substituting the normalized distance value by D_M for the distance value. For the second type of joint histogram, the number of bins was set to 20 for each value.

For the representation of the nodule surrounding region, we compute the absolute value (F) of the inner product between MPV and GV fields at each voxel in surrounding region of the nodule. Then, we represent the nodule surrounding by using the joint histogram of the distance value from the nodule surface and the absolute value of the inner product. To select the part of cylindrical or conic structures in the surrounding region, we specified two threshold values T_{SH}..for the shape index value (SH) and then obtained the region consisting of voxels which satisfied with a condition of $SH < T_{SH}$. The value of T_{SH} was set to 0.5. This process means that the surface types of cylindrical or conic structures are extracted by the shape index value. Two types of joint histogram are computed for the selected region in the similar equation of the computation the joint histogram of the CT density value and the distance value.

2.3 Similarity measure for retrieving lesions

It is a possible way to directly apply a similarity measure to the 3-D nodule image. However, this approach requires solving the registration between two images. In this study, we apply a simple similarity measure, which is the correlation coefficient (CC) to the nodule representation based on the joint histogram.

$$CC = \frac{\sum_{n=1}^{B_1}\sum_{m=1}^{B_2}(H_1(n,m)-\overline{H}_1)(H_2(n,m)-\overline{H}_2)}{\sqrt{\sum_{n=1}^{B_1}\sum_{m=1}^{B_2}(H_1(n,m)-\overline{H}_1)^2\sum_{n=1}^{B_1}\sum_{m=1}^{B_2}(H_2(n,m)-\overline{H}_2)^2}} \quad (3)$$

where $\overline{H}_1$ and $\overline{H}_2$ are the mean value of the joint histograms, H_1 and H_2, respectively.

At the first glance of a given nodule image, it is thought of that the nodule size and nodule density are important indexes for the visual assessment. Then, the features with respect to the local intensity structure are examined in detail to search similar patterns. In this study, we generate the list of similar nodule image by the searching process based on the similarity. We apply the similarity measure to the joint histogram of the CT density value and the distance value and then sort the *CC* value from more to less of similar patterns.

2.4 Difference Measure for Classifying Nodule Patterns

We select respectively the M examples from each list of the malignant and benign similar pattern to construct local two malignant and benign clusters that are similar to the indeterminate case concerning the CT density distribution pattern and the nodule size. The second type of the joint-histogram is used to model the distributions of the retrieved malignant and benign examples. Each malignant and benign example is represented by two 20x20 pixel images of the joint histograms regarding the shape index and F values and treated as 800-dimensional feature vector space. The Mahalanobis distance is used as a distance measure between the indeterminate pattern and each local model. In this preliminary study, we classify the indeterminate case into the cluster with small Mahalanobis distance.

3 Experimental Results

We considered the benign and malignant nodules shown in Fig. 1 as indeterminate cases and applied our approach to these cases.

Fig. 2 presents the first joint histogram-based representations of the malignant and benign cases shown in Fig. 1. Compared malignant with benign cases, it is observed that there is a few difference pattern between the joint histogram based representations with respect to CT density and distance except for the different expansion along the distance axis. While, it can be observed that there are difference patterns of the joint histogram-based representations concerning the shape index and the F value. Compared the malignant case with the benign case, the benign case has extremely high frequency of the shape index value around zero. This means that peak surface type occupies the inner structure of the benign case. Owning to the component of vessels and speculations, it seems that malignant case has larger amount of the component radiating from the nodule than the benign case.

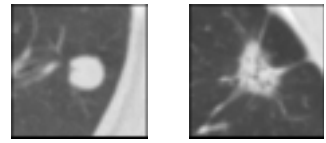

(a) (b)

Fig. 1. ROI slice images including benign and malignant nodules. (a) Benign case. (b) Malignant case.

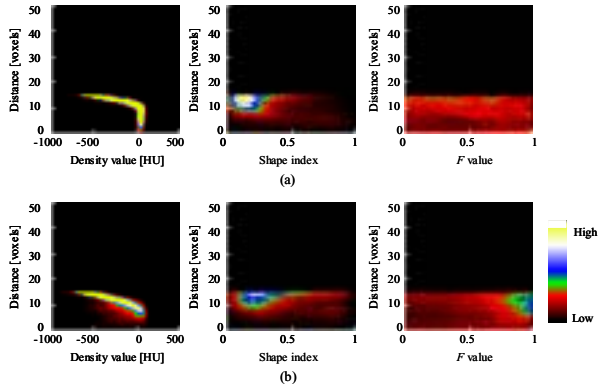

Fig. 2. Joint histogram-based representations of the malignant and benign cases shown in Fig. 1. (a) Benign case. (b) Malignant case. From left to right, representation with respect to the CT density value, shape index value, and *F* value, respectively.

Fig. 3 presents the searching similar images of the indeterminate cases shown in Fig.1 (a). This figure shows sorting results of similar images obtained from benign and malignant groups in our database. Fig. 4 presents the joint histogram-based representations of the most similar benign and malignant nodules to the indeterminate case. Compared these results with the representation result of the indeterminate case shown in Fig.2 (a), it can be observed that the indeterminate nodule pattern is similar to the benign one shown in Fig.4 (a). The Maharanobis distance of the indeterminate case was more close to the benign cluster. Fig. 5 presents the searching similar images of the indeterminate cases shown in Fig.1 (b). Fig. 6 presents the joint histogram-based representations of the most similar benign and malignant nodules to the indeterminate case. Compared these results with the representation result of the indeterminate case shown in Fig.2 (b), it can be observed that the indeterminate nodule pattern is similar to the malignant one shown in Fig.6 (b). The Maharanobis distance of the indeterminate case was more close to the malignant cluster.

4. Conclusion

We have presented an example-based assisting approach for classifying pulmonary nodules in 3-D thoracic CT images. The main idea is to formulate the nodule-classification problem as one of learning to recognize nodule patterns from examples.

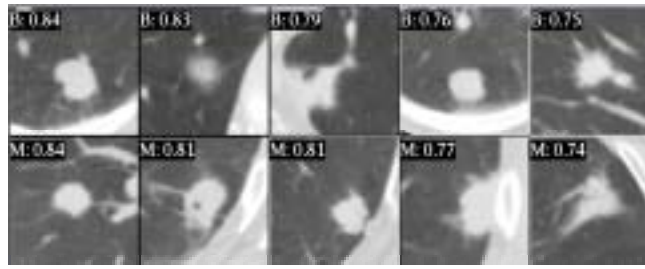

Fig. 3. Similar image of the case shown in Fig.1 (a). First row: similar image obtained from the benign group (B). Second row: similar images obtained from the malignant group (M). From left to right: sorting result from more to less similar pattern. The fraction number denotes the *CC* value in Eq. (3).

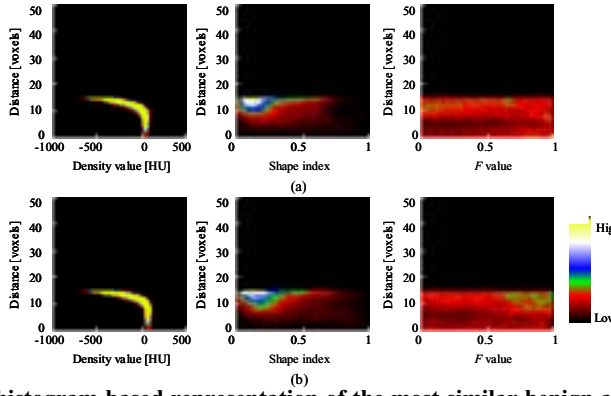

Fig. 4. Joint histogram-based representation of the most similar benign and malignant patterns of the case shown in Fig. 1(a). (a) Most similar benign pattern. (b) Most similar malignant pattern. From left to right, representation with respect to the CT density value, shape index value, and *F* value, respectively.

We have presented the application results of the searching similar images for an indeterminate nodule and then estimated the likelihood of the malignancy by computing the difference between representation patterns of the indeterminate case and the retrieved lesions. More research requires building a classifier between malignant and benign cases based on the similar patterns feature spaces. Still, we believe that the searching similar image approach would provide a better understanding for any given nodule in assisting physician's diagnostic decisions.

References

[1] M. Kaneko, K. Eguchi, H. Ohmatsu, R. Kakinuma, T. Naruke, K. Suemasu, N. Moriyama : Peripheral lung cancer: Screening and detection with low-dose spiral CT versus radiography. Radiology, vol.201 (1996) 798-802.

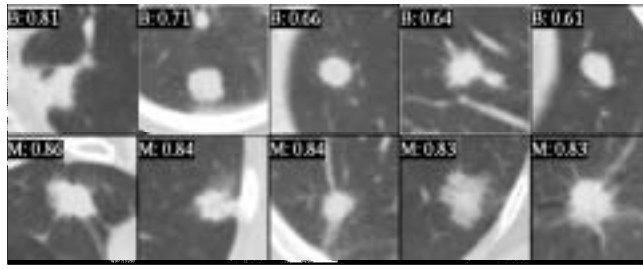

Fig. 5. Similar image of the case shown in Fig.1 (b). First row: similar image obtained from the benign group (B). Second row: similar images obtained from the malignant group (M). From left to right: sorting result from more to less similar pattern. The fraction number denotes the *CC* value in Eq. (3).

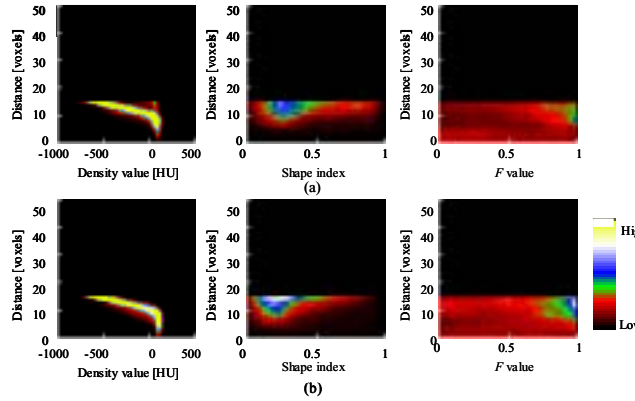

Fig. 6. Joint histogram-based representation of the most similar benign and malignant patterns of the case shown in Fig. 1(b). (a) Most similar benign pattern. (b) Most similar malignant pattern. From left to right, representation with respect to the CT density value, shape index value, and *F* value, respectively.

[2] Y. Kawata, N. Niki, H. Ohmatsu, R. Kakinuma, K. Eguchi, M. Kaneko, N. Moriyama : Quantitative surface characterization of pulmonary nodules based on thin-section CT images. IEEE Trans. Nuclear Science, vol. 45 (1998) 2132-2138.
[3] J.-P, Thirion and A. Gourdon : Computing the differential characteristics of isointensity surfaces. Computer Vision and Image Understanding, vol.61 (1995) 190-202.
[4] J. J. Koenderink and A. J. V. Doorn : Surface shape and curvature scales. Image and Vision Computing, vol.10 (1992) 557-565.
[5] Y. Kawata, N. Niki, H. Ohmatsu : Curvature based internal structure analysis of pulmonary nodules using thoracic 3-D CT images. IEICE Trans., vol.J-83-D-II (2000) 209-218.
[6] T. Saito and J. Toriwaki : Euclidean distance transformation for three-dimensional digital images. Trans. IEICE, vol.J76-D-II (1993) 445-453.
[7] C. Xu and J.L. Prince : Snake, shape, and gradient vector flow. IEEE Trans. Image Processing, vol. 7 (1998) 359-369.